

# Studies on fast electron transport in the context of fast ignition

Dimitri Batani

**Abstract.** This paper deals with the problem of fast electron propagation in plasmas, in the context of the fast ignition (FI) approach to inertial confinement fusion (ICF). In FI, a short-pulse high-intensity laser beam should generate a beam of relativistic electrons, which propagate into the compressed pellet, depositing energy and igniting the fuel. The study of electron propagation in dense matter is hence essential to the success of this scheme. The propagation of relativistic electrons in dense matter is determined by collisions of fast electrons with ions and electrons in the material, which can be described in terms of stopping power, but it also depends on self-generated magnetic and electric fields, which play a major, or even dominant role. In this paper we will show the importance of such collective effects by discussing several experimental examples.

**Key words:** inertial confinement fusion (ICF) • fast ignition (FI) • fast electrons • ultra-high-intensity lasers • relativistic laser-plasma interaction

## Introduction

The ICF relies on the use of laser beams (the direct drive approach) or soft X-rays (the indirect drive approach) to reach the conditions needed for ignition of the nuclear fusion reaction [12]. In ICF, the conditions for ignition of the D-T fuel (the well known Lawson's criterion) may be written as  $\rho R > 3 \text{ g/cm}^2$  and  $T \approx 5\text{--}10 \text{ keV}$ , where  $\rho R$  is the total areal density of the pellet (spherical target) at the stagnation time, i.e. at the time of maximum implosion. Achieving these conditions requires first the use of synchronized laser pulses irradiating the target with spherical symmetry (typically at intensity  $I \approx 10^{14} \text{ W/cm}^2$  within  $\approx 10 \text{ ns}$ ) to compress the fuel. Then the coalescence of a spherical shock wave in the centre may be used to create a central hot spark where the ignition conditions are satisfied; thermonuclear reactions initiated in this spark generate a thermonuclear combustion wave which rapidly propagates through the rest of target fuel.

This scenario was named as “isobaric approach” because the pressure in the very dense and relatively cold fuel is approximately equal to the pressure in the still low density, but very hot central spark.

The ignition has to be initiated by a small “spark” because heating the whole fuel to thermonuclear temperatures would require huge amounts of energy, dramatically reducing the possible energy gain.

The fact that it is possible to compress the targets to the density required for ICF ( $\rho \approx 500$  to  $1000 \times$  the den-

D. Batani  
Dipartimento di Fisica “G. Occhialini”,  
Università di Milano Bicocca,  
Piazza della Scienza 3, I-20126 Milano, Italy,  
Tel.: +39 02 6448 2313, Fax: +39 02 6448 2585,  
E-mail: batani@mib.infn.it

Received: 25 August 2010  
Accepted: 15 October 2010

sity of liquid DT) was shown already in the 1980's with experiments on the GEKKO XII laser in the Institute of Laser Engineering at the University of Osaka (Japan) [1]. Unfortunately, the neutron yields obtained in these experiments were much smaller than expected, implying that the central hot spot was not being generated.

In fact the main problem of the “classical” approach to ICF is that the non-uniformity in the laser irradiation (or in the target itself) produces a non-uniform compression, which leads to the deformation of the target and ultimately makes it impossibility to drive a converging spherical shock wave all the way to the centre of the fuel pellet. A simple one-dimensional (1D) model of the target implosion is sufficient to show that in order to reach a final target deformation of the order of  $\Delta R/R_{\text{final}} \approx 50\%$  (which is optimistically assumed as an upper limit), the fluctuations in the laser intensity irradiation have to be below 1% [15]. The actual situation may even be worse because the non-uniformities may act as seeds for the development of the Rayleigh-Taylor hydrodynamic instability.

The concept of “fast ignition” [17] is an alternative, relatively new approach to ICF, in which the compression and ignition phases of ICF are separated. The ignition is no longer initiated by the compression, so the constraints on the uniformity may be relaxed. In FI, we first have a “normal” compression with ns laser pulses, followed by an ultra-high-intensity pulse – generated using the “chirped pulse amplification” (CPA) technique – which creates a beam of relativistic electrons propagating through the external layers of the DT pellet and depositing their energy in a “lateral” hot spot, which is heated to the required temperature. (By the lateral hot spot we mean a hot region that most likely will not coincide with the geometrical centre of the imploding target, but would be located closer to the region directly irradiated by the high-intensity laser). The relation between the central hot spot ignition and the FI is to some extent similar to that of a diesel engine compared to a gasoline engine (which requires an external spark to ignite the fuel). We may also consider the FI pulse as an additional heating mechanism, similarly to what happens in the magnetic confinement fusion.

We can very simply calculate the required parameters for the ignition beam. Indeed we want to heat to the temperature of about 10 keV a region of typical radius  $R = 10 \mu\text{m}$  (the range of  $\alpha$  particles produced by DT fusion reactions), in the fuel compressed to 1000 times the solid density. The number of D and T ions contained in this volume is given by

$$(1) \quad N_{\text{DT}} = \frac{4}{3} \pi R^3 n_{\text{DT}} = 4 \times 10^{-9} \text{cm}^3 \times 10^{26} \text{cm}^{-3} = 4 \times 10^{17}$$

and, since each ion must attain a temperature of about 10 keV, the total energy we must deposit is about 10 kJ.

Also, in order to match the required propagation distance [17], we must generate electrons with a typical energy of  $\approx 1\text{--}2 \text{ MeV}$ , which requires a laser beam of intensity  $I_L \approx (1\text{--}2) \times 10^{19} \text{ W/cm}^2$ , known to produce electrons having such energies [5]. The required pulse duration is therefore

$$(2) \quad t_L = \frac{E}{\pi R^2 I_L} = 10 \text{ ps}$$

In this context it is therefore clear why we are interested in the problem of fast electron propagation, and in particular in assessing the importance of collisional effects vs. effects of (self-generated) electric and magnetic fields in their propagation.

The subject is also interesting from the point of view of basic plasma physics and an extensive research has been done on this subject in the last 10 years (for a review see [4]). It is also of crucial importance for the optimization of novel laser-driven protons sources [8, 11, 13, 16], where protons are accelerated by the fields created by the fast electron current on target rear side.

### Conversion efficiency and mean energy

The feasibility of FI fusion rests on several key suppositions. The first is that the laser energy will be converted into fast electrons at the 20–40% efficiency level for intensities higher than  $10^{19} \text{ W/cm}^2$ . This conjecture has indeed been largely proven in experiments done over the last 10 years. Figure 1 shows experimental results obtained with two different laser systems: the PW laser at the Lawrence Livermore National Laboratory (LLNL) (empty dots) [10] and the 100 TW laser at the Laboratoire pour l'Utilisation des Lasers Intenses (LULI) [14]. Results from several other laboratories show similar trends and reveal the absolute conversion efficiency of the same order. The efficiency at which the laser pulse energy is converted into fast electrons seems to scale approximately as the intensity of the laser to the power of 1/4 [7] (of course this is expected to saturate around  $10^{21} \text{ W/cm}^2$ ).

Note that the efficiency appears to depend only upon the intensity, not on the laser pulse duration. Also, the results at LULI were obtained after conversion of laser to  $2\omega$  ( $0.53 \mu\text{m}$ ) against the fundamental harmonics used at LLNL. Interestingly, within experimental error bars, no clear dependence on the laser wavelength is observed. This is a quite surprising result, since the conversion to  $2\omega$  results in a higher critical density and a strong improvement of contrast, hence implying the reduction of a prepulse and thereby a strong reduction of the preplasma.

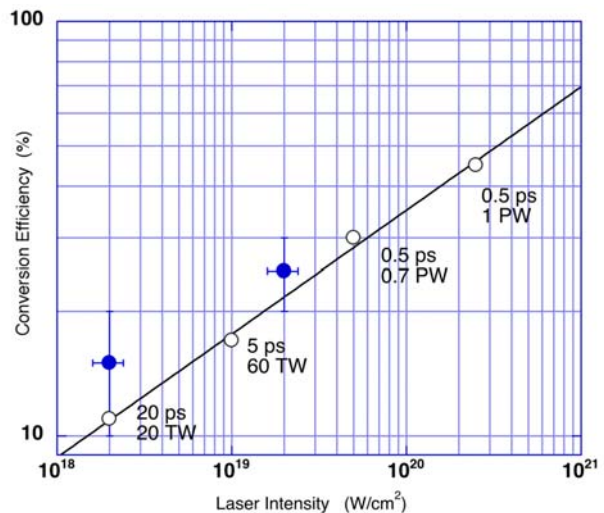


**Fig. 1.** Experimentally measured conversion efficiency  $\eta$  of the laser energy into fast electrons, as a function of the laser intensity. Empty circles indicate LLNL ( $1\omega$ ), full circles LULI ( $2\omega$ ).

Let's also note that despite the fact that results obtained in several laboratories are similar, they should be treated with caution: indeed, the absolute numbers depend to some extent on parameters which are not always measured (for example the fraction of the laser energy that is actually focused on the target, the fraction of the laser pulse energy that is really contained in the nominal focal spot, etc.). Results are then often obtained only by using some *reasonable* but *untested* assumptions.

Finally, the conversion efficiency into fast electron energy is obtained by performing a numerical integration over the whole fast electron energy distribution. Again, since this distribution is usually measured only in few points, or in the energy range above certain threshold, the extrapolation to low electron energies is necessary, giving another factor of incertitude.

The second important point, which affects the feasibility of fast ignition, is the scaling of the electron mean energy (usually called “fast electron temperature” in the literature) vs. laser intensity. There has been considerable work confirming the heuristic relationship between the laser intensity and the fast electron energy. In general, the scaling law  $T_{\text{fast}} \propto (I_L \lambda^2)^b$  is found to hold. Measurements have been performed with 1.06  $\mu\text{m}$  laser light, 0.53  $\mu\text{m}$  light (second harmonic) and 0.8  $\mu\text{m}$  light (Ti:Sa lasers). As for the exponent, it was found that  $b \approx 1/3$  for “lower” laser intensities, and  $b \approx 1/2$  for “higher” laser intensities.

The factor 1/3 may be theoretically related to resonant absorption [5], giving in practical units

$$(3) \quad T_{\text{fast}} \approx 100 \text{ keV } (I_L \lambda^2)^{1/3}$$

where  $I_L$  is expressed in units of  $10^{17} \text{ W/cm}^2$  and the wavelength  $\lambda$  is in microns. On the other hand, the exponent 1/2 is explained as a consequence of the ponderomotive scaling [19]

$$(4) \quad T_{\text{fast}} \approx 512 \text{ keV } [(1 + 0.073 (I_L \lambda^2))^{1/2} - 1]$$

The transition in the type of behaviour takes place around  $10^{19} \text{ W/cm}^2$ . The two scaling laws are shown in Fig. 2, together with a number of experimental results. For intensities of the order of  $(2-3) \times 10^{19} \text{ W/cm}^2$ , the mean energy of the distribution of hot electrons is ap-

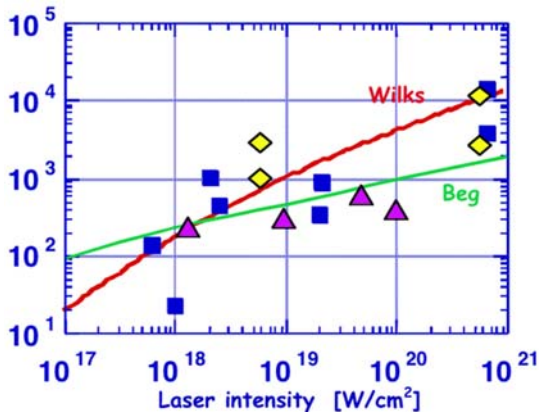


**Fig. 2.** Measured fast electron temperatures vs. laser intensity, compared to resonant absorption and ponderomotive scaling. Blue squares – data obtained at UCRL; yellow diamonds – data from electron spectra; triangles – LULI data from  $K_\alpha$  penetration.

proximately 0.5 MeV, which is predicted to match the required propagation range of ICF targets (i.e. about 200 to 300  $\mu\text{m}$  between the critical density  $n_c$  and the compressed fuel where the electron density is  $\approx 10^4 n_c$  [17]).

Let's notice that another key parameter of the fast electron beam is its divergence. Indeed, if the divergence is not negligibly small, then even if the region where fast electrons are produced is 10  $\mu\text{m}$  in size, the beam cross section may dramatically increase before it reaches the dense core. For larger heated volume the amount of the laser energy that has to be delivered to the target dramatically increases, since we still need to reach the  $\approx 10 \text{ keV}$  temperature.

### Collisional effects vs. collective effects in propagation

The propagation of fast electrons in matter is governed on one side by collisional effects (usually expressed through the stopping power of electrons in the material), and on the other side by collective (i.e. electromagnetic) effects.

Local charge neutrality requirements play a dominant role in the physics taking place in the medium that the fast electrons are assumed to traverse. Charge neutrality arises from the intense micro fields within the plasma: a return current  $j_{\text{return}}$  balancing the *incoming* fast electron current  $j_{\text{fast}}$  is needed to allow fast electron propagation and sets up practically instantaneously. The matter has to respond in a very short time. In an ideal plasma the response time is given by  $t = 1/\omega_p$ , where  $\omega_p$  is the plasma frequency, while in a resistive material it is given by  $t = \epsilon_0/\sigma$ . In both cases, this time is much shorter than 1 fs. For electrons travelling nearly at the speed of light in vacuum, the maximum thickness of the non-neutral part of the fast electron beam is given by  $ct \leq 0.1 \mu\text{m}$ , an entirely negligible distance.

The problems related to current balance and charge neutrality have first been discussed by Bell *et al.* [6]: in order to allow penetration, we must have  $j_{\text{total}} = j_{\text{fast}} + j_{\text{return}} \approx 0$  at all points within the target. In high density matter, the return current is generated from the background thermal plasma and hence  $j_{\text{return}}$  is affected directly by the resistivity of the material. An Ohmic potential is established within the material and its gradient is an electric field whose direction slows the fast electrons down. We can express this by introducing an Ohmic stopping scale length  $z_0$  over which the potential change is equal to the mean energy of the fast electrons. The scale length depends upon (a) the mean energy of the fast electrons, (b) the number of fast electrons produced by the laser, and (c) the average value of the resistivity. According to Bell *et al.*

$$(5) \quad z_0 = 3 \times 10^{-3} (kT_{\text{fast}})^2 \sigma_6 (\eta I_{17})^{-1} \mu\text{m}$$

where  $\sigma_6$  is the plasma conductivity in units of  $10^6 (\Omega \cdot \text{m})^{-1}$ ;  $kT_{\text{fast}}$  is the electron temperature in keV;  $I_{17}$  is the laser intensity in units of  $10 \text{ W/cm}^2$ , and where  $\eta$  denotes the efficiency of the laser energy to fast electron energy conversion. Bell's law may simply be found by equating the work done by the electric field over the distance  $z_0$  to the initial kinetic energy of fast electrons (of the order of  $kT_{\text{fast}}$ ), i.e.

$$(6) \quad eEz_0 = kT_{\text{fast}}$$

and by recalling that  $j_{\text{fast}} \approx j_{\text{return}}$ . The return current is related to the electric field  $E$  by Ohm's law ( $j_{\text{return}} = \sigma E$ ) while the direct fast electron current is given by  $j_{\text{fast}} = n_e ce$  (the fast electron practically moving at the speed light in vacuum). Now the total number of produced fast electrons is

$$(7) \quad N_e^{\text{tot}} \approx \frac{\eta E_L}{kT_{\text{fast}}}$$

from which follows

$$(8) \quad j_{\text{fast}} = n_e ce = \frac{N_e^{\text{tot}}}{\pi R^2 ct_L} ce = \frac{\eta I_L e}{kT_{\text{fast}}}$$

By equating this to  $j_{\text{return}} = \sigma E$ , we obtain the Bell's law.

The concept of Ohmic stopping length is an indicator of whether a particular experimental measurement is being dominated by collective or collisional mechanisms. For example, in measurements where the number of fast electrons generated is relatively large, but either (1) the material is not already sufficiently hot or compressed enough to have driven the resistivity vs. temperature dependence towards the "Spitzer" limit; or (2) the peak intensity of the laser is not sufficiently high to produce a high value of the mean fast electron energy, the Ohmic stopping length  $z_0$  is likely to be much shorter than attenuation distance produced by collisions (the collisional penetration range as determined by the stopping power).

Conversely, in experiments where the total number of fast electrons is relatively small, or the target material is already in the Spitzer limit, and the peak intensity of the laser is high enough to produce a large value of the mean fast electron energy, the Ohmic stopping length is expected to be long enough so as not to play a significant role in the fast electron transport.

Also, let's notice that the stopping power increases when  $Z$  and  $\rho$  increase while electric inhibition decreases when  $\sigma$  increases. Hence, using targets going for instance from CH to Al, Cu and Au, the stopping power would be increasing, while the electric inhibition would be decreasing. Hence many experiments may simply fall in a regime where they are not able to see electric effects. This is for instance the case of the experiments realised at Rutherford with the Vulcan laser facility [5].

## Experimental results

The first observation of a difference in fast electron penetration in conductors and insulators was probably contained in Key and Wharton's papers [9, 18]. A clearer experiment showing the difference between insulators and conductors, and the role of electric inhibition in insulators, was performed by Pisani *et al.* [14] with the LULI 100 TW CPA laser. A 350 fs full width at half maximum (FWHM) 0.53  $\mu\text{m}$  laser pulse with an energy up to 20 J was focused by a  $f/3$  off-axis parabola at normal incidence onto the target up to  $10^{19} \text{ W/cm}^2$ . Frequency doubling of the laser beam al-

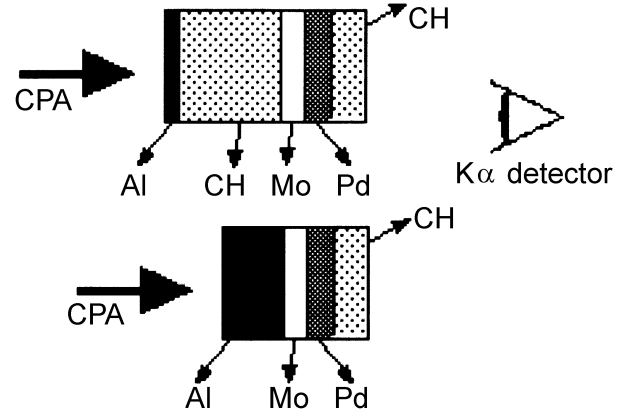


**Fig. 3.** The principle of the electron penetration experiment conducted at LULI.

lowed a contrast ratio better than  $10^8:1$ . Targets shown in Fig. 3 were used to compare fast electron penetration in metals and insulators and determine the importance of electric inhibition. After the propagation layer (Al or CH), the fast electrons reach two layers of fluorescent materials (20  $\mu\text{m}$  of Mo and 20  $\mu\text{m}$  of Pd) where they produce  $K_{\alpha}$  photons, which are detected by a charge coupled device (CCD) camera used in a single shot mode to allow spectroscopic analysis. A fourth 50  $\mu\text{m}$  plastic layer on the rear side of the target avoided any spurious  $K_{\alpha}$  emission. By changing the thickness of the propagation layer it was possible to obtain the penetration depth of fast electrons in the given material. In order to assure the same interaction conditions, even with plastic targets the first layer was 1.2  $\mu\text{m}$  Al. Hence any difference in experimental  $K_{\alpha}$  yield was only due to differences in electron propagation through the solids, and not to a different number or temperature of the produced fast electrons.

Two series of shots were done in which the laser intensity was changed by varying the focusing conditions. In the first series, the focal spot diameter was  $\approx 30 \mu\text{m}$  and the intensity was  $(1-2) \times 10^{18} \text{ W/cm}^2$ , while in the second the spot was  $\leq 10 \mu\text{m}$  and the intensity  $(1-2) \times 10^{19} \text{ W/cm}^2$ . By comparing the predictions of Monte Carlo (MC) simulations and the experimental ratio of  $K_{\alpha}$  yield of palladium and molybdenum vs. the target thickness, the temperature of fast electron in the two cases was obtained: respectively  $\approx 180 \text{ keV}$  and  $\approx 400-500 \text{ keV}$ , compatible with Beg's law [5]. This comparison was performed in the case of Al targets, where electric effects were small.

Figure 4 shows the experimental  $\text{MoK}_{\alpha}$  emission as a function of the crossed thickness (in  $\mu\text{m}$ ) for both plastic and aluminium targets, in the high intensity case ( $(1-2) \times 10^{19} \text{ W/cm}^2$ ). An exponential fit to the results gave the following values for penetration depth:  $230 \pm 40 \mu\text{m}$  for Al and  $180 \pm 30 \mu\text{m}$  for CH. On the other hand, computer simulations based on collisional models yielded  $235 \pm 10 \mu\text{m}$  and  $690 \pm 20 \mu\text{m}$  respectively (assuming a 400 keV temperature). We see that the number obtained from simulations for Al is compatible with the experimental result, while in the case of plastic there is a large discrepancy, showing a strong inhibition. A similar situation is found in the low intensity case.

Hence this experiment showed again the importance of electric field effects. Moreover, at lower laser

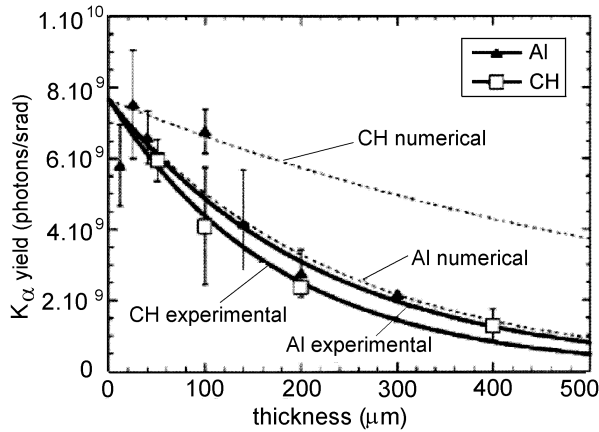


**Fig. 4.** Results obtained at LULI in the high intensity case ( $T_{\text{hot}} \approx 400$  keV): experimental and numerical  $K_{\alpha}$  yield vs. target thickness in  $\mu\text{m}$ , and interpolation (exp  $(-R/R_0)$ ).

intensity ( $(1-2) \times 10^{18}$  W/cm<sup>2</sup>) the penetration in plastic was found to be the same, if not increased (being  $220 \pm 50$   $\mu\text{m}$ , see Fig. 5). This result cannot be explained by collisional models; indeed at lower intensities the fast electron temperature is lower (180 keV), and therefore the penetration should be smaller. Qualitatively, this is easily explained by Bell's law. Indeed, the electric penetration  $z_0$  is inversely proportional to the laser intensity and the conversion efficiency  $\eta$  (which also increases with the laser intensity). In other words, electric inhibition increases with laser intensity so that it will result in no increase, or even a reduction, of penetration. In this case it is then correct to speak about an *electric-field-limited fast-electro-transport*.

Let's notice that in the limiting cases of negligible collisions and very high laser intensities (for which the Wilks' scaling of the fast electron temperature holds), the two exponents in the Bell's law cancel each other, yielding a penetration range which is totally independent of fast electron energy. Such an "unnatural" behaviour (at least if one thinks in terms of collisional stopping power) again constitutes a proof of the importance of collective effects.

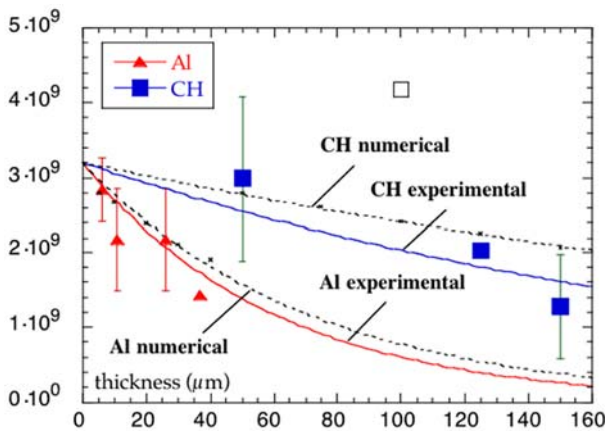


**Fig. 5.** Comparison of Al and CH penetration at an intensity of  $2 \times 10^{18}$  W/cm<sup>2</sup>. The CH shows a shorter range than predicted by collisional theory, while Al is consistent with collisional stopping. When the intensity is increased to  $2 \times 10^{19}$  W/cm<sup>2</sup>, the collisional theory predicts a range of over 700  $\mu\text{m}$ , while the experimental value remains equal to that observed at  $2 \times 10^{18}$  W/cm<sup>2</sup>, approximately 220  $\mu\text{m}$ .

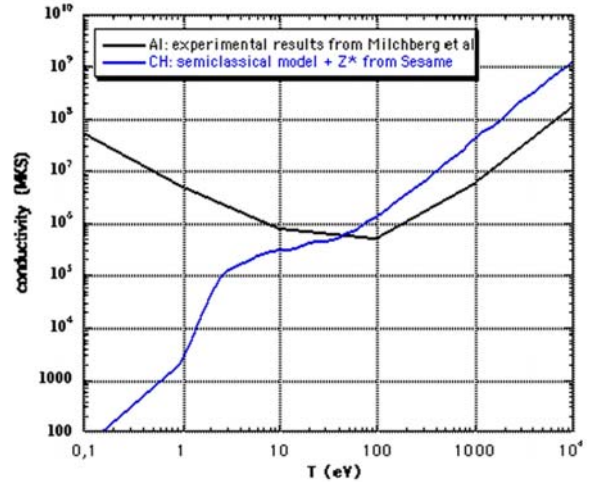


**Fig. 6.** Comparison of the conductivity of a typical metal (Al) with that of an insulator (plastic), vs. temperature.

### Dependence of propagation on electrical conductivity

The general behaviour of the conductivity of all materials is schematized in Fig. 6, where the conductivity of a typical metal (Al) is compared with that of an insulator (plastic), at various temperatures. In metals the conductivity is decreasing, and it reaches a minimum (the saturated value of resistivity, or the Ioffe-Rigel limit) when the electron mean free path becomes equal to the inter-ionic distance. Beyond that limit, which corresponds to temperatures close to the Fermi energy of metals, conductivity rises again because the material is becoming a plasma and begins to follow the Spitzer's law (i.e. that  $\sigma$  is proportional to temperature to the 3/2 power).

The behaviour of insulators is quite different. Starting from very low values of  $\sigma$ , there is an initial increase, which is driven by ionization of the background material due to the temperature effect (collisional ionization, Saha-like distributions). Again, at temperatures of the order of few 10 eV, such behaviour changes to the Spitzer-like.

This initial phase in insulators is sometimes neglected. However it can be important in the interpretation of several contemporary experiments (as already explained in the previous sections).

The graph in Fig. 6 was obtained for constant density, equal to the initial mass density of the material. This is usually appropriate for the fast heating induced by fast electrons (isochoric conditions).

The behaviour of conductivity in gases and in foams made of insulating materials is similar to that of insulators, but in this case the initial density of the material is a parameter which can be easily changed. Also, due to their lower density, a given energy deposition from fast electrons corresponds to a larger increase in temperature. Therefore such materials reach the Spitzer-regime more easily, which simplifies the analysis of experimental results.

### Propagation in gases

In order to further investigate the question of propagation of fast electrons, and of propagation inhibition,

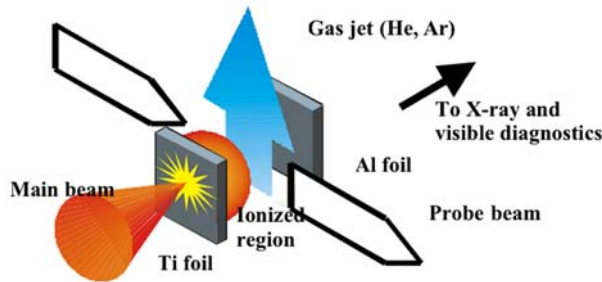


**Fig. 7.** Experimental set-up of Batani *et al.* experiment [2] in which the fast electrons are produced in a conductor by the ultra-intense laser, and then are propagated across a region which has a controlled density of gas. The gas is neutral, and has the density at which even if ionized, the equivalent “background” electron density is less than the density of fast electrons injected into the volume.

a few experiments (for instance [2]) used gas targets. Here, the density of the background material could be reduced below the density of foams, with the additional advantage that gases are transparent, unlike foams or many types of solids, allowing the use of such diagnostic tools as optical shadowgraphy. This allows fast electron propagation to be studied *within* the target and *continuously* in time. The experimental set-up used in this kind of experiment is shown in Fig. 7.

Figure 8 shows some typical shadowgraphy images, displaying a large cloud and straight lines probably connected to *electron jets*. Such jets could be due to the *first* generation of fast electrons, arriving to the rear of the first foil and propagating into the gas before a large field has developed (their presence is thereby not too important in fast electron transport, since the cloud contains the majority of electrons).

In the conditions of the experiment, the propagation of the majority of the fast electrons across the volume is greatly inhibited, and their velocities become sub-relativistic. The ionization rate and the collisional rate depend upon the density of the gas, and when the ionization occurs, more of the generated fast electrons make their way across the volume in a “cloud-like” structure. As a result, the propagation distance (measured as the size of the cloud) increases both with time and with the density of the background gas.

The propagation of fast electrons in the gas is limited by the need for a neutralizing return current, and by

the creation of electrostatic fields due to charge separation. The condition on the current neutralization of fast electrons and the return current,  $j_{\text{tot}} = en_b v_b - en_e v_e \approx 0$ , implies that i) the maximum fast electron current density which can propagate is  $en_e c$ , and ii) background electrons are also accelerated to high velocities in our conditions (which means that the distinction between *fast* and *slow* electrons is no longer valid). Also, charge neutrality can be violated at the leading edge of the propagation only, over a distance of the order of the Debye length  $\lambda_D$  of fast electrons. This is also the region where the space charge electric field is large and can ionize the background gas, and this coincides with the width of the ionization front  $\Delta x$ . Such an electric field very rapidly ionizes the background gas, creating the free electrons needed for the neutralizing return current. Finally, free electrons are set in motion and establish a return current which cancels the fast electron current. The establishment of the return current and the cancellation of the positive charge left behind by the fast electrons takes a time of the order of  $\approx \lambda_D/v_e$ , where  $v_e$  is the drift velocity of background electrons. This process is slow because the free background electrons are (at least initially) slow and strongly collisional, and collisions inhibit the return current. However, since no further propagation of the fast electrons is possible before the charge separation is cancelled, the fast electron current is finally forced to move with a velocity close to the return velocity of background electrons, i.e.  $v_{\text{cloud}} \approx v_e$ . This gives a slow velocity and a strongly inhibited propagation.

Experiments on fast electron propagation in gases are also interesting because they provide a direct evidence for very strong electric fields associated with fast electron propagation, e.g. by using proton radiography [3]. This is a recently developed diagnostics, which relies on laser-generated protons as a point-like source for backlighting, used to get radiographic images (point projection imaging) of the gas on a stack of radiochromic films. Let’s notice that in principle proton radiographic images may be obtained either by relying on the mass difference in the crossed path (different proton absorption) or on the deflection of protons due to fields.

In the present case, we studied the propagation of fast electrons in gases which, due to their low mass den-

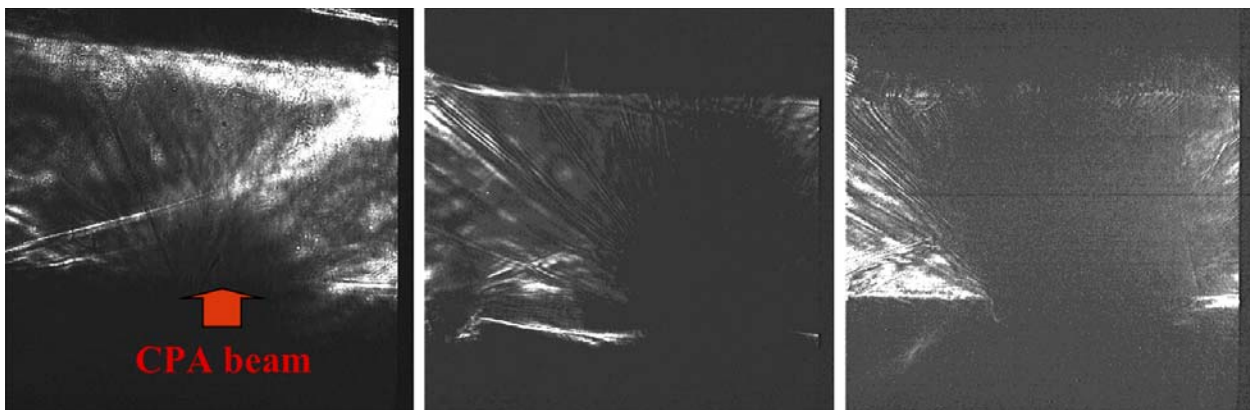


**Fig. 8.** Shadowgraphy time series obtained with an Ar gas jet at 70 bar (gas atomic density:  $2.7 \times 10^{19} \text{ cm}^{-3}$ ) and laser intensity  $\approx 4 \times 10^{19} \text{ W/cm}^2$ . By changing the delay between the CPA beam and the probe beam we can reconstruct the evolution of the electron cloud. The images correspond to  $t_0$ ,  $t_0 + 4 \text{ ps}$ , and  $t_0 + 13 \text{ ps}$ . The red cross shows the position where the CPA laser beam is focused.

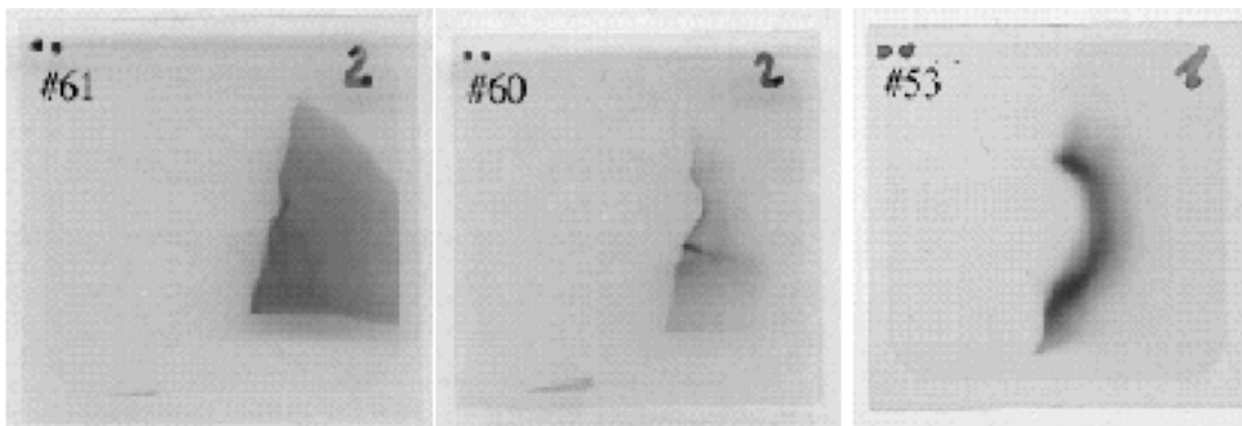


**Fig. 9.** Proton radiography images obtained with  $N_2$  gas at pressures of 15, 30, and 100 bars. The dimension of the images, taking into account magnification, is about 2 mm. All images correspond to a time of about 20 ps after the arrival of the main laser beam on the electron target (i.e. they are formed by protons with about 3 MeV energy).

sity, are completely transparent to energetic protons, so that proton trajectories can be altered by fields only. Let's also notice that proton radiography is sensitive to quasi-static fields only, the rapidly oscillating fields (at laser or plasma frequency) being averaged out in time. This is indeed the case of the electrostatic fields produced by charge separation, which are thought to be important in fast electron propagation in gases.

Figure 9 shows some typical proton radiography images [3]. We clearly see a hemispherical shape, more pronounced at 100 bars than at 15 or 30 bars. This indeed demonstrates the presence of a very strong electrostatic field, located at the ionization front, which affects the trajectories of protons. In this case the background gas pressure ( $N_2$ ) has been changed, showing an increased penetration for the higher pressure, in agreement with the shadowgraphy results. Also, the size of the region is in qualitative agreement with shadowgraphy results.

## Conclusions

In this paper we have given some examples of experiments and analyses related to the understanding of how very large currents of relativistic electrons are transported through materials. As discussed in the introduction, a complete understanding of the physics of this electron transport is essential to the prospects for "fast ignition".

There is ample evidence that ultra-high intensity lasers will produce large quantities of energetic ( $\geq 1$  MeV) electrons at an efficiency that can exceed 30% for intensities of the order of  $10^{19}$  W/cm<sup>2</sup>. This is good news for the FI approach to ICF.

However, the fast electron penetration into dense materials is not simply a function of their binary collisions with ions, but rather is more often constrained by electrostatic forces arising from the necessity of localized charge neutrality. Indeed, one of the surprising aspects of the recent experimental results is that the fast electron penetration is a strong function not only of the density of the material, but of its conductivity, and, more surprisingly, of  $t$  relative magnitude of the generated fast electron density compared to the density of unbound electrons in the target material.

The study of very high current transport has thus proven to be much more complicated than originally anticipated. This may provide very nice physics, but it shows that the route to FI is not paved with gold.

**Acknowledgment.** The author wishes to acknowledge the discussions and the precious collaboration of S. Baton, F. Pisani, J. Davies, M. Koenig, L. Gremillet, C. Rosseaux, T. Hall, D. Neely, K. Lancaster, V. Malka, M. Manclossi, J. Santos, F. Canova, V. Tikhonchuk, M. Lontano, M. Key, S. Wilks, R. Stephens, F. Beg, M. Veltcheva, P. Carpeggiani, H. Stabile, R. Dezulian, A. Bernardinello, J. Honrubia, F. Berez, B. Vauzour, and please forgive me if I forgot anybody!

## References

1. Azechi H, Jitsuno T, Kanabe T *et al.* (1991) High-density compression experiments at ILE, Osaka. *Laser Part Beams* 9:193–207
2. Batani D, Baton SD, Manclossi M *et al.* (2005) Ultra-intense laser-produced fast electron propagation in gas jst. *Phys Rev Lett* 94:055004/1–055004/4
3. Batani D, Baton SD, Manclossi M *et al.* (2009) Laser-driven fast electron dynamics in gaseous media under the influence of large electric fields. *Phys Plasmas* 16:033104/1–033104/5
4. Batani D, Freeman R, Baton S (2007) Review of experimental results on electron transport in laser-plasma interactions. In: Yamanouchi K (ed) *Progress in ultrafast intense laser science*. Springer, Berlin
5. Beg F, Bell AR, Dangor AE *et al.* (1997) A study of picosecond laser-solid interactions up to  $10^{19}$  W cm<sup>-2</sup>. *Phys Plasmas* 4:447–457
6. Bell A, Davies JR, Guerin S *et al.* (1997) Fast-electron transport in high-intensity short-pulse laser – solid experiments. *Plasma Phys Control Fusion* 39:653–659
7. Freeman RR, Batani D, Baton SD *et al.* (2006) The generation and transport of large currents in dense materials: the physics of electron transport relative to fast ignition. *Fusion Sci Technol* 49:297–315
8. Kaluza M, Schreiber J, Santal MIK *et al.* (2004) Influence of the laser prepulse on proton acceleration in thin-foil experiments. *Phys Rev Lett* 93:045003/1–045003/4
9. Key M, Cable MD, Cowan TE *et al.* (1998) Hot electron production and heating by hot electrons in fast ignitor research. *Phys Plasmas* 5:1966–1973

10. Koch JA, Key MH, Freeman RR *et al.* (2001) Experimental measurements of deep directional columnar heating by laser-generated relativistic electrons at near-solid density. *Phys Rev E* 65:016410/1–016410/8
11. Lindau F, Lundh O, Person A *et al.* (2005) Laser-accelerated protons with energy dependent beam direction. *Phys Rev Lett* 95:175002/1–175002/4
12. Lindl J (1995) Development of the indirect-drive approach to inertial confinement fusion and the target physics basis for ignition and gain. *Phys Plasmas* 2:3933–4024
13. Malka V, Faure J, Fritzier S *et al.* (2006) Production of energetic proton beams with lasers. *Rev Sci Instrum* 67:03B302/1–03B302/3
14. Pisani F, Antonicci A, Bernardinello A *et al.* (2000) Experimental evidence of electric inhibition in the propagation of fast electrons in solid matter. *Phys Rev E* 62:R5927–R5930
15. Skupsky S, Craxton RS (1999) Irradiation uniformity for high-compression laser-fusion experiments. *Phys Plasmas* 6:2157–2163
16. Snavely RA, Key MH, Hatchett SP *et al.* (2000) Intense high-energy proton beams from Petawatt. *Phys Rev Lett* 85:2945–2948
17. Tabak M, Clark DS, Hatchett SP *et al.* (2005) Review of progress in fast ignition. *Phys Plasmas* 12:057305/1–057305/8
18. Wharton K, Hatchett SP, Wilks SC *et al.* (1998) Experimental measurements of hot electrons generated by ultraintense ( $> 10^{19}$  W/cm<sup>2</sup>) laser-plasma interactions on solid-density targets. *Phys Rev Lett* 81:822–825
19. Wilks SC, Kruer WL, Tabak M *et al.* (1992) Absorption of ultra-intense laser pulses. *Phys Rev Lett* 69:1383–1386